Matter and Radiation at Extremes | RESEARCH ARTICLE | pubs.aip.org/aip/mre

Featured

Characterization of bright betatron radiation generated by direct laser acceleration of electrons in plasma of near critical density

Cite as: Matter Radiat. Extremes 9, 027201 (2024); doi: 10.1063/5.0181119
Submitted: 14 October 2023 • Accepted: 16 January 2024 •
Published Online: 7 February 2024

J. Cikhardt,[1,a)] M. Gyrdymov,[2] S. Zähter[3,4] P. Tavana[2] M. M. Günther,[3] N. Bukharskii[5,6] N. Borisenko,[6] J. Jacoby,[2] X. F. Shen,[7] A. Pukhov,[7] N. E. Andreev[8,9] and O. N. Rosmej[2,3]

AFFILIATIONS

[1] Faculty of Electrical Engineering, Czech Technical University in Prague, 16627 Prague 6, Czech Republic
[2] Goethe University, Frankfurt, Max-von-Laue-Straße 1, 60438 Frankfurt am Main, Germany
[3] GSI Helmholtzzentrum für Schwerionenforschung GmbH, Planckstraße 1, 64291 Darmstadt, Germany
[4] Focused Energy GmbH, Im Tiefen See 45, 64293 Darmstadt, Germany
[5] National Research Nuclear University MEPhI, Kashirskoe shosse 31, 115409 Moscow, Russian Federation
[6] Lebedev Physical Institute RAS, Leninskiy Prospekt 53, 119991 Moscow, Russian Federation
[7] Heinrich-Heine-University Düsseldorf, Universitätsstrasse 1, Düsseldorf, Germany
[8] Joint Institute for High Temperatures, RAS, Izhorskaya st. 13, Bldg. 2, 125412 Moscow, Russian Federation
[9] Moscow Institute of Physics and Technology, Institutskiy Pereulok 9, 141700 Dolgoprudny, Russia

[a)] **Author to whom correspondence should be addressed:** cikhajak@fel.cvut.cz

ABSTRACT

Directed x-rays produced in the interaction of sub-picosecond laser pulses of moderate relativistic intensity with plasma of near-critical density are investigated. Synchrotron-like (betatron) radiation occurs in the process of direct laser acceleration (DLA) of electrons in a relativistic laser channel when the electrons undergo transverse betatron oscillations in self-generated quasi-static electric and magnetic fields. In an experiment at the PHELIX laser system, high-current directed beams of DLA electrons with a mean energy ten times higher than the ponderomotive potential and maximum energy up to 100 MeV were measured at 10^{19} W/cm^2 laser intensity. The spectrum of directed x-rays in the range of 5–60 keV was evaluated using two sets of Ross filters placed at 0° and 10° to the laser pulse propagation axis. The differential x-ray absorption method allowed for absolute measurements of the angular-dependent photon fluence. We report 10^{13} photons/sr with energies >5 keV measured at 0° to the laser axis and a brilliance of 10^{21} photons s^{-1} mm^{-2} mrad^{-2} (0.1%BW)$^{-1}$. The angular distribution of the emission has an FWHM of 14°–16°. Thanks to the ultra-high photon fluence, point-like radiation source, and ultra-short emission time, DLA-based keV backlighters are promising for various applications in high-energy-density research with kilojoule petawatt-class laser facilities.

I. INTRODUCTION

Laser-driven sources of synchrotron-like (betatron) radiation are characterized by very short time duration, small size, directed emission, and extreme brightness.[1] Thanks to these qualities, such radiation sources are promising for a number of advanced applications, such as high-resolution x-ray radiography and absorption spectrometry of ultra-fast processes (e.g., in inertial confinement fusion[2]), shock wave and implosion research,[3–6] medicine,[7,8] and biology.[9,10]

The betatron radiation generated in the interaction of a femtosecond laser pulse with gas jets or gas cells of under-critical density ($\leq 10^{19}$ cm^{-3}) is caused by electrons accelerated in the process of laser wake field acceleration (LWFA). Typically, these accelerated

electrons approach energies of the order of hundreds of MeV and total charges of 10–100 pC.[11–17] In the case of well-optimized schemes, multi-GeV energies[18–20] and >nC charges can be reached.[21,22] The efficiency of the betatron radiation can be significantly enhanced by novel methods such as tailoring the laser temporal shape and the target density profile.[18,23] Increasing the plasma density and/or laser pulse duration at relativistic laser intensity can lead to a self-modulated regime of acceleration (SMLWFA),[24–26] where the laser pulse is substantially longer than the period of the Langmuir electron oscillations. In this regime, the charge of the accelerated electrons, and therefore the number of photons emitted, increases by more than an order of magnitude compared with LWFA. Measurements of the betatron radiation generated in the self-modulated LWFA regime at the sub-ps sub-kJ Titan laser system have been reported in Refs. 2 and 27. Simulations performed under the 1.1 kJ sub-ps PETAL conditions showed that the SMLWFA regime predicts up to 8×10^{11} photons with energy 2–60 keV.[28]

The experimental study on the generation of betatron radiation using sub-ps laser pulses presented in this work is motived by predictions of 3D particle-in-cell (PIC) simulations with the Virtual Laser Plasma Lab (VLPL) code.[29–31] These simulations show that efficient production of betatron radiation can be achieved by interacting the laser with a plasma of near-critical electron density (NCD) $n_C \approx 10^{21}$ cm^{-3} for a wavelength of 1054 nm formed from an ionized low-density foam (2–3 mg/cm^3).[31,32]

In contrast to the gas targets commonly used for various goals, we have found relatively few works dealing with low-density foam targets, examples being experiments on the Vulcan,[33,34] OMEGA,[35] and Titan[36] laser facilities. These experiments dealt with electron and proton acceleration in plasmas of density $0.9n_c$ to $90n_c$ (3–300 mg/cm^3 foam), but not with the generation of betatron radiation. A major contribution to the study of the relativistic laser interaction with foam targets has been made at the PHELIX laser facility, where directed beams of super-ponderomotive electrons and MeV gamma-ray emissions (in the case of combinations of foams with high-Z converters) have recently been obtained with record-breaking conversion efficiencies.[37–40] In these experiments, the foam targets with a density of 2–3 mg/cm^{-3} were pre-ionized by a ns pulse and irradiated by a laser pulse of 750 ± 250 fs duration and (2–5) × 10^{19} W/cm^2 intensity. Thanks to the efficient direct laser acceleration (DLA) process,[12,13] super-ponderomotive electrons (>2 MeV) with an effective temperature of ≥13 MeV carried charge of the order of μC and reached energies up to 100 MeV.[37,38] This experimental result is in good agreement with 3D-PIC simulations.[37,38,41] The exact characterization of the electron acceleration, including the absolute spectra and the angular distribution of electron fluence, allowed a theoretical study of betatron radiation to be performed that was tailored for the experiments on PHELIX.[31,32] This study predicted betatron radiation reaching 7×10^{11} photons in the 1–30 keV energy range and a brilliance of ~10^{20} photons s^{-1} mm^{-2} mrad^{-2} (0.1%BW)$^{-1}$. These values are comparable to the photon number and brilliance expected on PETAL at laser energy and intensity an order of magnitude higher than in the case of PHELIX.[28] The combination of ultra-high photon fluence and high brilliance makes DLA-based betatron radiation sources very promising for high-energy-density research with kJ PW-class lasers characterized by high background radiation.

In this paper, we present the first experimental measurement of the betatron radiation driven by the interaction of a sub-ps laser pulse laser with pre-ionized low-density polymer foam targets.[37,42]

The structure of the remainder of the paper is as follows: The experimental setup, parameters of the laser beam, information about the target, and a detailed description of the diagnostics can be found in Sec. II. Experimental data, a discussion, and results, including the betatron radiation spectra, are presented in Sec. III. Finally, conclusions are summarized in Sec. IV.

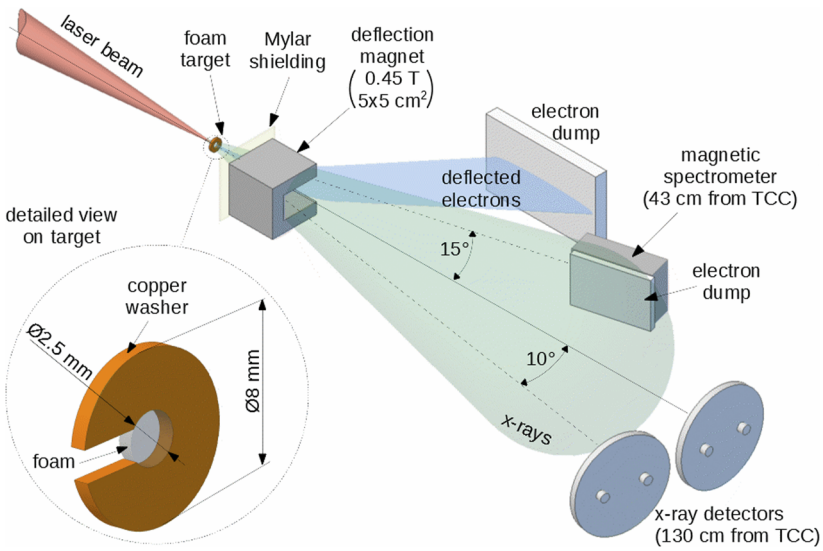

FIG. 1. Schematic of experimental arrangement.

II. EXPERIMENTAL ARRANGEMENT

The experiment was performed on the PHELIX laser facility at the GSI Helmholtz Centre for Heavy Ion Research in Darmstadt, Germany. PHELIX is a PW-class Ti:sapphire/Nd:glass hybrid laser system with a fundamental wavelength of 1054 nm.[43] A schematic of the experimental arrangement is shown in Fig. 1.

As targets, we used low-density (2–3 mg/cm^{-3}) polymer foams with a diameter of 2.5 mm and a thickness of 300–1500 μm.[42] For technological reasons, the foam was grown inside a copper washer with inner and outer diameters of 2.5 and 8 mm, respectively. By full ionization of the foam, we obtained a plasma with an electron density $n_e \approx 0.64 \times 10^{21}$ cm^{-3} that is near the critical density $n_c \approx 10^{21}$ cm^{-3} for the laser wavelength of 1054 nm. In our experiments, the foam was ionized by a well-defined ns laser pulse with a full energy 0.2–2 J, a pulse length of 3 ns, and an intensity in the range of 10^{13}–10^{14} W/cm^2. The ns pulse initiated an ionization wave propagating with a velocity of (1–2) $\times 10^7$ cm/s. After a 3 ns delay, when the ionization wave penetrated about 300–600 μm depth, the formed NCD plasma was irradiated by the main laser pulse of 750 ± 250 fs duration, 60–80 J energy measured before the compressor, and a ns amplified spontaneous emission (ASE) contrast of 10^{11}. Both the laser pre-pulse and main pulse were focused on the target by a 150 cm off-axis parabolic mirror to the focal spot with the FWHM of 15 μm containing an energy $E_{FWHM} \approx 17$–20 J. Thus, the intensity in the focal spot approached (1–2) $\times 10^{19}$ W/cm^2. To prevent reflection of the laser beam back to the laser system, the target normal was tilted by 3°–10° with respect to the optical axis. To reduce the influence of protons and ions emitted from the target on the betatron radiation diagnostics, a Mylar foil was placed behind the target, in the direction of the laser beam. Behind the Mylar shielding, at a distance of 20 mm from the target, a C-shaped magnetic yoke with a pair of neodymium magnets was placed to deflect the accelerated electrons to a massive plastic dump. The magnetic yoke was shielded by 10 mm of plastic to prevent the generation of bremsstrahlung that could interfere with the betatron radiation signals. The mean magnetic field within the yoke working gap was ~0.45 T. To monitor high-energy (tens of MeV) electrons that were not efficiently deflected, we used a magnetic spectrometer placed at 15° to the laser axis at a distance of 59 cm from the target.

Since the betatron radiation produced by DLA electrons in an NCD plasma is assumed to be well directed,[31] we used two detectors placed at a distance of ~130 cm at 0° and 10° to the laser axis. The detectors consisted of a set of x-ray filters, two layers of MS-type image plates (IPs), and a semiconductor photodiode AXUV HS11. A detector is shown in Fig. 2.

Regarding the set of filters, we used two kinds: "thin" and "thick." Both filter sets allowed us to evaluate the x-ray spectra by the differential absorption method. In the case of the "thin" filters, we used the Ross method.[44,45] The Ross method utilizes filter foils made of different materials with thicknesses optimized to reach as similar transmission characteristics as possible so that they differ only by the K-edge energy. Thus, a difference in signals obtained behind paired Ross filters corresponds to the number of photons with energy in the range given by the K-edge energies, i.e., the difference in the transmission characteristics. In this manner, it is possible to obtain an x-ray spectrum with a relatively high resolution in the photon energy (~1 keV). For cases in which the difference between signals behind paired Ross filters would be insufficient and lead to large uncertainty in the number of photons, in addition to the Ross pair, a supplementary filter was used to obtain a filter triplet.

The supplementary filter was made of Mylar or aluminum foil with an optimized thickness making the low-energy region around the K-edge peak negligible in the transmission characteristics. Consequently, as in the classical Ross method, the photon energy interval was given by the transmission characteristics difference, but only one filter had the K-edge transmission peak. Thus, on the one hand, we obtained worse resolution in the spectrum, but on the other hand, the signal-to-background level was higher. In addition to the differential filters, the thin filter set also included 70 μm thick silver foil with a significant K-edge peak in the region of ~13–25 keV. Transmission characteristics of the filters based on the data from Refs. 46 and 47 are presented in Fig. 3 and the differential transmission characteristics representing the individual channels of the spectrometer can be seen in Fig. 4.

In the case of the "thick" filter set, we also utilized the differential absorption method, but owing to the relatively large thickness, the peaks around the K-edges in the transmission characteristics were negligible. We used aluminum and copper filters with six

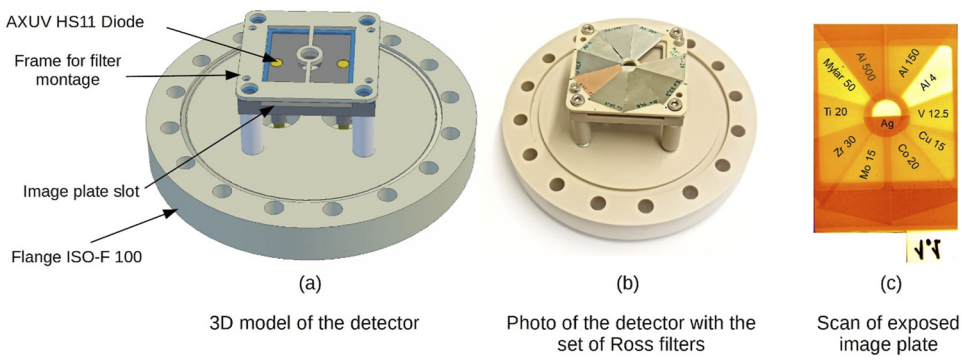

(a) 3D model of the detector

(b) Photo of the detector with the set of Ross filters

(c) Scan of exposed image plate

FIG. 2. X-ray detector. (a) 3D model of detector. (b) Photograph of prepared detector with a set of Ross filters. (c) Example of image plate signal, where the individual filters are labeled by the foil material and thickness in micrometers.

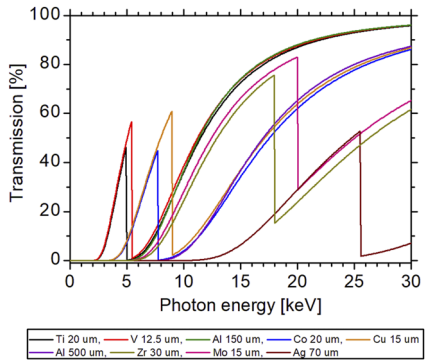

FIG. 3. Photon transmission characteristics of thin filters.

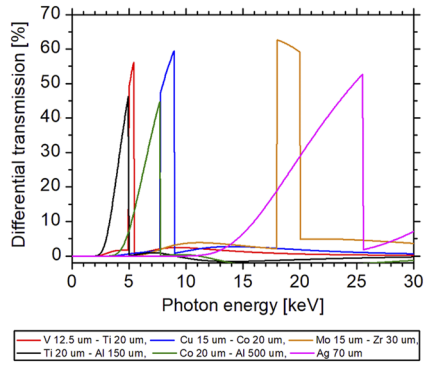

FIG. 4. Differential photon transmission characteristics of thin filter pairs.

various thicknesses to obtain a six-channel spectrometer. The transmission characteristics of the thick filters based on the data from Ref. 48 and the differential absorption characteristics for the individual spectrometer channels are displayed in Figs. 5 and 6, respectively. It is obvious that the "thick" filters have lower spectral resolution and can be applied to the restricted photon range (>10 keV), but on the other hand they absorb eventual ions that could interfere with the betatron radiation signal better than the "thin" filters, and also this set allows measurement of the spectrum at higher photon energies than in the case of the thin filters.

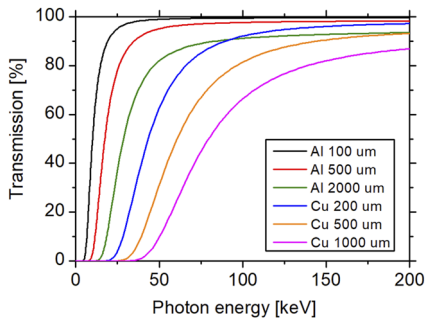

FIG. 5. Photon transmission characteristics of thick filters.

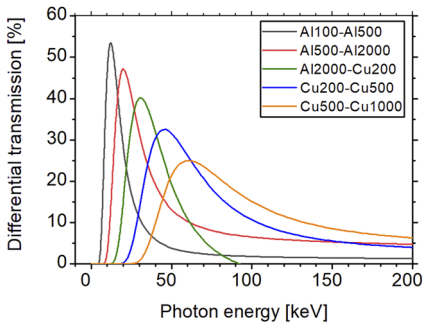

FIG. 6. Differential photon transmission characteristics of thick filter pairs.

As mentioned above, the betatron radiation was detected by IPs in our experiment. The first IP layer 40 × 40 mm^2 was located right behind the filters. This IP layer was followed by a 0.5 mm thick copper filter, which transmitted 1% of ~30 keV radiation, and the second IP layer of identical dimensions that served as a monitor of the radiation background caused by fast electrons (>20 MeV), which were not deflected by the magnet. Small windows for the AXUV HS11 semiconductor diode were cut both in the IPs and in the copper filter. This diode is sensitive to photons in the keV energy range, with a time response of 0.7 ns[49,50] Thanks to the time resolution provided by the diode, we could obtain information about protons and ions that penetrated through the Mylar shielding, magnetic field, and Ross filters to the IP detector and interfered with the betatron radiation signal. Thus, with the help of the diode signal, we optimized the thickness of the Mylar shielding to efficiently stop the protons and ions and minimize their effect on the measured betatron radiation.

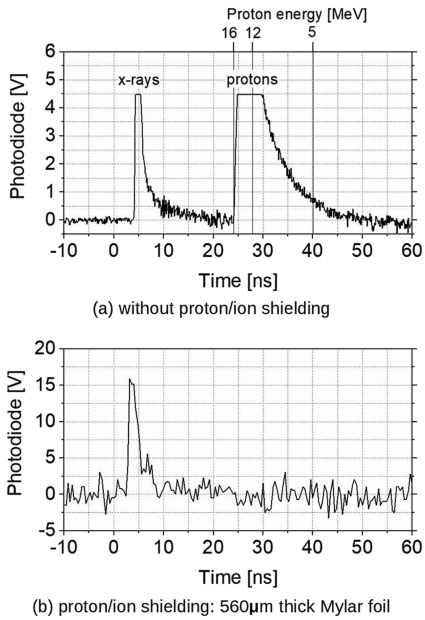

FIG. 7. Examples of semiconductor diode signal: (a) without proton/ion shielding; (b) with proton shielding by 560 μm thick Mylar foil.

Examples of the diode signal from shots on a pre-ionized 2 mg/cm^3 foam of 560 μm thickness without the Mylar shielding and with optimized Mylar shielding are shown in Figs. 7(a) and 7(b), respectively. We note that the proton peak in Fig. 7(a) is relatively high, and, using the time-of-flight method, we can evaluate the proton energies, which can reach up to 16 MeV.

We assume that such a relatively efficient acceleration of protons occurs when the rear side of the foam target remains in a solid state after the action of the ns pulse that creates the conditions for target normal sheath acceleration (TNSA). In contrast to x-rays, the impact of protons or ions produces extremely high signals on the IPs and makes it impossible to recognize betatron radiation in the x-ray detector data. This is shown in Fig. 8, where the contribution of protons completely dominates the signals from the Ross filter spectrometer when the shielding is not applied. For this reason, we evaluated the x-ray spectra only in the shots in which protons were not observed in the diode signal.

Thanks to the well-known absorption characteristics of Mylar foils,[46,47] the influence of the proton shielding on the x-ray transmission can be corrected. The IP signal is given by

$$s = \int \frac{\mathrm{d}\Phi}{\mathrm{d}E} T_F(E) T_S(E) \eta(E)\, \mathrm{d}E, \tag{1}$$

where Φ is the photon fluence, T_F and T_S are transmissions of the particular filter and proton shielding, respectively, E is the photon energy, and $\eta(E)$ is the IP sensitivity. Thus, the measured x-ray spectra are evaluated by differences of IP signals behind the filter pairs in individual spectrometer channels:

$$\frac{\mathrm{d}\Phi}{\mathrm{d}E} \cong \frac{S_A - S_B}{\Delta E_{AB} \langle T_F \rangle_{AB} \langle T_S \rangle_{AB} \langle \eta \rangle_{AB}}, \tag{2}$$

where S_A and S_B are IP signals of the paired IPs in photostimulated luminescence events (PSL) per unit surface, and ΔE_{AB} is the energy window given by the width of differential transmission characteristics (see Figs. 4 and 6). The photon transmissions $\langle T_F \rangle_{AB}$ and $\langle T_S \rangle_{AB}$ are average values with respect to ΔE_{AB}. The average IP sensitivity $\langle \eta \rangle_{AB}$ is given by the calibration published in Ref. 51. The uncertainty of this calibration is ~15%. As far as the filters are concerned, verification by the MicroProf system in the target laboratory of GSI[52] showed that the deviation in the thickness was less than 10%. Considering other factors such as nonideal overlap of the paired filters' transmission characteristics outside the sensitive region and uncertainty of scanning, we calculate that the total uncertainty in the evaluation of photon fluence is about 50%. As far as the uncertainty in the energy is concerned, we determine it as the FWHM of the window in the differential absorption characteristic for the particular spectrometer channel.

III. RESULTS AND DISCUSSION

This section is devoted to evaluation and discussion of the experimental results. The interaction of the relativistic laser pulse with the NCD plasma leads to intense emission of particles and radiation, which makes analyses of IP and diode signals difficult, since these detectors are sensitive to both radiation and particles. In the case of the diode time-resolved signals, the situation is easier, since it is possible to resolve between radiation on the one hand and protons and ions on the other using the time-of-flight method. However, with this method, we cannot distinguish between photons and relativistic electrons, and their contributions to the diode signal must be discussed.

The electrons emitted from the rear side of the target are partially deflected by the 0.45 T magnetic field of the yoke with permanent magnets behind the target (see Fig. 1). However, the measurement with magnetic spectrometers at an angle of 15° shows a significant number of electrons with energy above 30 MeV that were not efficiently deflected: see the electron energy spectrum in Fig. 9. This 30 MeV energy limit is in accordance with the deflection angle given by[53]

$$\sin\left(\frac{\varphi}{2}\right) = \frac{e}{2\gamma\sqrt{2mE_e}} \left\| \int \mathbf{B} \times \mathrm{d}\mathbf{l} \right\|, \tag{3}$$

where φ is the electron deflection angle, e is the electron charge, γ is the Lorentz factor, m is the electron rest mass, E_e is the electron energy, $\mathbf{B}$ is the magnetic field, and $\mathrm{d}\mathbf{l}$ is an element of length. See the dependence of deflection angle on electron energy displayed in Fig. 10.

Thus, the high-energy electrons (>30 MeV), which are not sufficiently deflected, enter the diode and interfere with the x-ray signal. Fortunately, the fluence of >30 MeV electrons is much smaller than the expected fluence of the >15 keV x-ray photons,[31,32] and considering the diode response to electrons and x-rays,[49,50] the influence

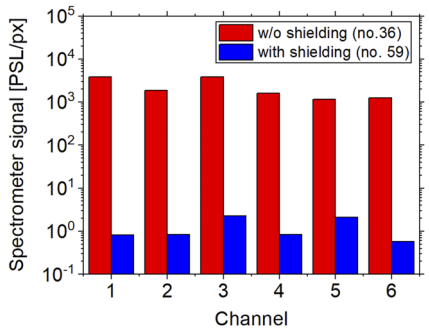

FIG. 8. Example of outputs from individual channels of the Ross filter spectrometer in shots with and without proton/ion shielding.

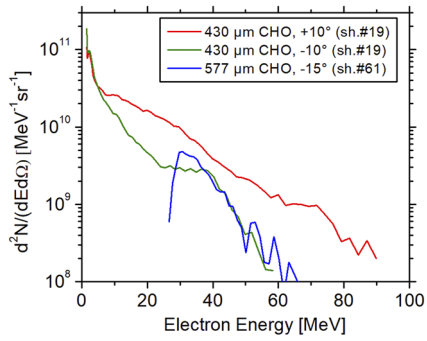

FIG. 9. Electron spectra from shots without (red and green) and with (blue) the deflection magnetic field.

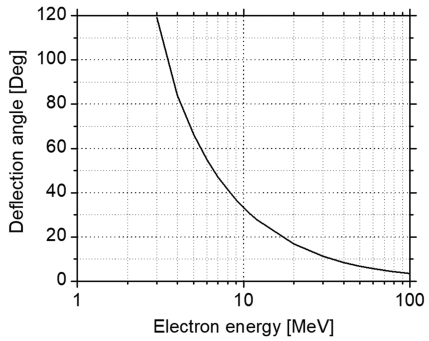

FIG. 10. Deflection of electrons by the magnetic yoke as a function of electron energy.

of electrons on the diode signal should be negligible in comparison with that of x-rays. The amplitude of the x-ray signal carries information about the x-ray production efficiency. In Table I, we compare x-ray signal amplitudes in terms of their dependence on the thickness of 2 mg/cm^3 CHO foam in shots with the same ns pulse (10^{13} W/cm^2, 3 ns duration) and 3 ns delay between the ns pulse and the sub-ps relativistic pulse of 10^{19} W/cm^2. The shielding in front of the x-ray detector (12.5 μm Ti and two IPs) transmits 10%–100% photons with energy above 15 keV. One can see that the maximum of the diode signal peaks at 800 μm and drops with further increase in foam thickness.

The diode signals also illustrate the influence of the ns-pulse intensity on x-ray production, as can be seen in Table II. In the case of 10^{14} W/cm^2 intensity, the amplitude of the detected signal is two to three times higher than at 10^{13} W/cm^2. The reason could be that at lower intensities, a larger fraction of the foam stays in the solid state, and thus the conversion of the laser energy into x-rays is weaker.

To demonstrate the efficiency of the x-ray emission by interaction of the laser beam with an NCD plasma, we present in Table III a comparison of the results obtained for foams with the results for solid foils of ~1 μm thickness. In Table III, the 0.9 μm Mylar and 400 μm CHO foam have the same areal density of 10 mg/cm^2, but very different origins of the x-rays: plasma self-radiation in the case of Mylar and 20 times more intense betatron radiation in the case of foam.

As far as the IP detectors are concerned, they are more sensitive to relativistic electrons than to x-rays,[54] and their contribution to the signal must be corrected. As mentioned in Sec. II, between the first IP layer and the second IP layer (background monitor) was a 0.5 mm thick Cu filter that was almost opaque for the keV betatron radiation but practically transparent for the >30 MeV electrons. We calculated the electron stopping in the first IP layer and the 0.5 mm Cu filter using a CASINO Monte Carlo simulation,[55] where the IP was modeled in accordance with Ref. 56. The simulation indicates that in the electron energy range 10–100 MeV, the IP and Cu filter slightly reduce the energy of incident electrons, but this change in the electron energy is negligible with respect to the IP electron response characteristics.[51] Therefore, we assume that the energies deposited by electrons in the first and second IP layers are equivalent. Thus, we can subtract the signal of the second IP layer (background monitor) from that of the first layer and exclude the effect of electrons on the result of the x-ray (betatron radiation) measurement. We should mention that the signal of the background monitor is not entirely homogeneously distributed over the whole IP surface: see the IP signals from the example shot in Fig. 11 (580 μm foam, 66 J). Therefore, from the first IP signal, we always subtract the background signal that corresponds to the same geometric position.

Another phenomenon that could interfere with the betatron radiation signal is the characteristic K-shell radiation and bremsstrahlung caused by electrons in the copper washer around the foam target. The answer to the question whether such undesired x-rays disturb our measurement could be given by the directionality of the measured radiation. Figure 11 shows IP signals in photostimulated luminescence (PSL) behind the set of thin filters placed at 0° and 10° to the laser axis. One can see that after subtraction of the background, the signals measured at 0° to the laser axis are three to four times higher than those measured at 10°. Since the K-shell radiation of a point-like source is generally considered to be isotropic, it cannot be the main origin of the detected x-rays. As far as bremsstrahlung is concerned, it usually has a strong maximum in

TABLE I. Dependence of x-ray (≥15 keV) signal amplitude on foam thickness for 10^{13} W/cm^2, 3 ns pulse and 10^{19} W/cm^2 main pulse with 3 ns delay. The x-ray diode shielding is 12.5 μm Ti and two IPs.

Shot	Target	ps-pulse energy (J)	X-ray pulse (V)
No. 36	Foam, 460 μm	71	~9
No. 42	Foam, 800 μm	70	16
No. 44	Foam, 1000 μm	75	7
No. 43	Foam, 1500 μm	70	3

TABLE II. Dependence of the x-ray (≥15 keV) signal amplitude on ns-pulse intensity: from 10^{13} W/cm^2 up to ~10^{14} W/cm^2 (duration 3 ns, delay 3 ns). The x-ray diode shielding is 12.5 μm Ti and two IPs.

Shot	Target	ns-pulse intensity (W/cm^2)	ps-pulse energy (J)	X-ray pulse (V)
No. 36	Foam, 460 μm	10^{13}	71	~9
No. 47	Foam, 400 μm	10^{14}	78	29
No. 44	Foam, 1000 μm	10^{13}	75	7
No. 46	Foam, 1000 μm	10^{14}	80	19

TABLE III. Dependence of x-ray (≥15 keV) signal amplitude on target material.

Shot	Target	ns-pulse intensity (W/cm^2)	ps-pulse energy (J)	X-ray pulse (V)
No. 47	Foam, 400 μm	10^{14}	78	29
No. 46	Foam, 1000 μm	3×10^{13}	80	19
No. 54	Mylar, 0.9 μm	No ns pulse	70	1.3
No. 56	Gold, 0.96 μm	No ns pulse	76	5

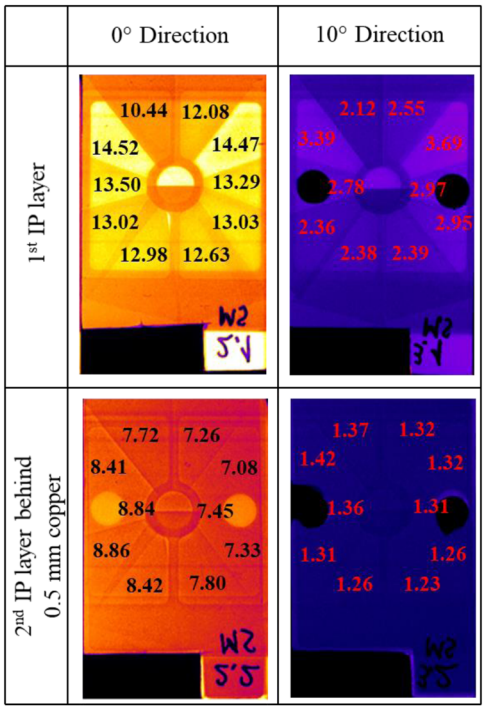

FIG. 11. Examples of IP signals behind the set of thin filters from the shot with 580 μm foam target and 66 J in the main pulse.

the direction of the incident relativistic electron beam.[57] Since the copper washer is oriented coaxially with respect to the laser axis, the only electrons that can generate bremsstrahlung must move in the direction transverse to the optical axis. Thus, the x-ray detectors are placed at angles of 80° and 90° with respect to the bremsstrahlung radiation maximum (corresponding to the direction from the focal spot to the inner wall of the copper washer: see Fig. 1). In these orientations, the bremsstrahlung intensity should exhibit a minimal dependence on the angle, a trend that contradicts the observed significant directivity. Moreover, at 80°, the bremsstrahlung intensity should be slightly higher than at 90°: a contrary trend to what we actually observe. Thus, we believe that the detected radiation is most likely of betatron origin, and we consider the measured x-ray spectra as spectra of the betatron radiation.

As an example of the spectra obtained with the help of the thin filters, we present a shot with a 580 μm thick foam target and total laser energy of about 66 J (≤20 J FWHM) in Fig. 12. The x-ray spectra measured at 0° and 10° are represented by the black and orange points, respectively. Their vertical errors are given mostly by the uncertainty in the IP scanning calibration and nonideal overlap of the paired filters' transmission characteristics outside the sensitive region, and the horizontal errors are given by the FWHM of the filter pair's photon energy bandwidth.

In Fig. 12, the data measured at 0° to the laser axis are fitted by an analytical function. According to the theory presented in Refs. 58 and 59, the spectrum of betatron radiation produced by a monoenergetic electron beam can be expressed by the formula

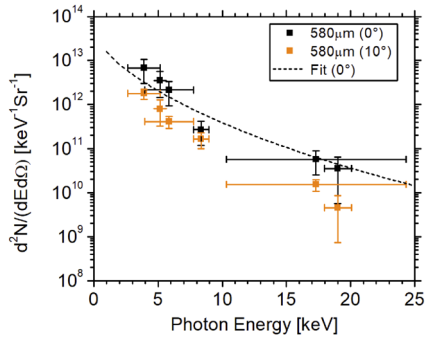

FIG. 12. Betatron radiation spectrum from a shot with a 580 μm thick foam target in the directions of 0° and 10°.

$$\frac{\mathrm{d}^2N(0^\circ)}{\mathrm{d}E\,\mathrm{d}\Omega} \cong N_\beta \frac{3e^2}{2\pi^3\hbar c\varepsilon_0}\gamma^2\frac{E}{E_{\mathrm{crit}}^2}\mathscr{K}_{2/3}^2\left(\frac{E}{E_{\mathrm{crit}}}\right), \tag{4}$$

where N_β is the number of betatron oscillations, γ is the Lorentz factor, and $\mathscr{K}$ is the modified Bessel function of the second kind. The critical energy of the betatron radiation can be calculated as $E_{\mathrm{crit}} = 3\hbar r_\beta \omega_\beta / c$, where r_β is the betatron oscillation amplitude, which is assumed to be comparable to the ion channel radius of approximately 10 μm, and ω_β is the betatron oscillation frequency.[58,59] Since, in our experiment, we have a broad range of electron energies, we consider a beam of electrons with energies 1–100 MeV and a one-temperature Maxwell–Boltzmann energy distribution $f_{MB}(E_e)$. Thus, the measured data at 0° are fitted by superposition of betatron spectra from all components' electron energies E_e:

$$\frac{\mathrm{d}^2N(0^\circ)}{\mathrm{d}E\,\mathrm{d}\Omega} \cong C\int_{E_e=1\,\mathrm{MeV}}^{100\,\mathrm{MeV}} N_\beta\gamma^2\frac{E}{E_{\mathrm{crit}}^2}\mathscr{K}_{2/3}^2\left(\frac{E}{E_{\mathrm{crit}}}\right)f_{MB}(E_e)\,\mathrm{d}E_e, \tag{5}$$

where C is a fitting constant. The second fitting parameter is the temperature of the electron beam. The best fit has been obtained for kT_e = 8 MeV, which is realistic for our experimental configuration.[38]

Whereas the spectrum in Fig. 12 obtained with the help of thin filters represents rather low x-ray energies of 4–18 keV, for the reconstruction of the spectrum in the higher-energy range of 12–60 keV, we use the set of thick filters. An example of such a spectrum from a shot with a 470 μm thick foam target is shown in Fig. 13. To fit the measured data in Fig. 13, we use the same function as in the case of Fig. 12. The best fit of the data measured by the thick filters in the higher-energy region of the spectrum is obtained for electron temperatures above 30 MeV, which indicates a two-temperature distribution.[38] Comparing the low-energy spectrum in Fig. 12 and the high-energy spectrum in Fig. 13, we can see that the spectra obtained with thin and thick targets are interconnected.

To compare the influence of shot parameters on the x-ray spectrum, we performed measurements with various target thicknesses and ns-pulse energies. In Fig. 14, we present spectra obtained with the help of the thin filters from the following shots: 470 μm foam, 3×10^{13} W/cm^2 ns pulse, and 64 J ps pulse (violet data points); red points: 580 μm foam, 1×10^{13} W/cm^2 ns pulse, and 66 J ps pulse (red data points); and 1500 μm foam, 1×10^{13} W/cm^2 ns pulse, and 83 J ps pulse (gold data points). Similarly, Fig. 15 displays spectra obtained using thick filters: 470 μm foam, 1×10^{13} W/cm^2 ns pulse,

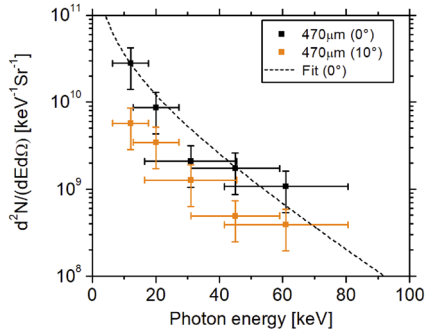

FIG. 13. Spectrum of betatron radiation in the directions of 0° and 10° evaluated with a help of thick filters.

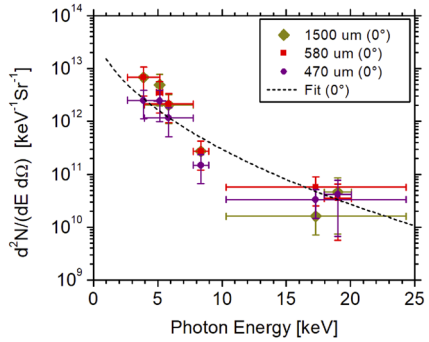

FIG. 14. X-ray spectra for different 2 mg/cm^3 foam thicknesses evaluated with the help of the thin filters set placed at 0° to the laser axis.

and 76 J ps pulse (blue data points); 890 μm foam, 1×10^{14} W/cm^2 ns pulse, and 76 J ps pulse (green data points). In all shots shown in Figs. 14 and 15, the intensity of the main pulse was ~10^{19} W/cm^2 and the delay between ns and sub-ps pulses was 3 ns. The spectra in both Figs. 14 and 15 were detected at a direction of 0° to the laser axis.

The difference in the photon fluence measured by means of the absorption method correlates well with the results from the x-ray diode presented in Tables I and II for photon energies >15 keV. At the same time, the accuracy provided by the filters is not enough to make a final conclusion.

Regardless of target thickness, the emission angle of the x-ray emission is relatively narrow (see Figs. 12 and 13). The x-ray radiation fluence in the direction of 0° is approximately three to four times higher than that in the direction of 10°. Assuming a Gaussian angular distribution of the radiation with its maximum in the direction of 0°, we obtain a half-angle at FWHM of about 7° (~100 mrad rms). Such a directionality is 2.7–3.6 times higher than the result of 3D-PIC calculations.[31,32] Knowing the directionality, we can obtain the spectrum of betatron photons emitted to all directions and compare it with the 3D-PIC simulation[31,32] (Fig. 16). As one can see, the measured spectral intensity above a photon energy of 5 keV is slightly lower than in the simulation, while in the region below 5 keV, the intensity is higher. This can be explained by the diagnostic uncertainties and some differences in the laser and plasma parameters between experiments and simulations.

Integrating the spectrum in Fig. 16 over the photon energy, we obtain a total number of photons (>5 keV) of ~3×10^{11} and a total radiated energy of about 0.32 mJ (which gives a conversion efficiency ~1.6×10^{-5}) that are in good agreement with the 3D-PIC simulations.[31,32] Such a betatron radiation yield is comparable to the simulation results for the interaction of a laser with a significantly higher energy of 1.1 kJ with a dilute plasma slab of 3 cm length.[28] Also, a comparison with the scaling of betatron radiation production from gas jets, presented in Ref. 60, shows that our betatron output in the 10–20 keV energy range corresponds to a laser power that is an order of magnitude higher than that in our experiment. As far as the brilliance is concerned, according to the simulations,[31,32] it reaches 3×10^{20} photons s^{-1} mm^{-2} mrad^{-2} (0.1%BW)$^{-1}$ for 5 keV photon energy. Since, in the experiment, we observed a similar number of emitted photons but an approximately three times narrower emission angle, we obtained for a 10^{19} W/cm^2 ps laser pulse an ultrahigh brilliance of the order of magnitude of 10^{21} photons s^{-1} mm^{-2} mrad^{-2} (0.1%BW)$^{-1}$ at 5 keV, assuming a pulse duration corresponding to a laser pulse of length 0.7 ps and a radiation source diameter of 4–5 μm caused by laser self-focusing in the NCD plasma (see the simulation results in Refs. 31 and 32).

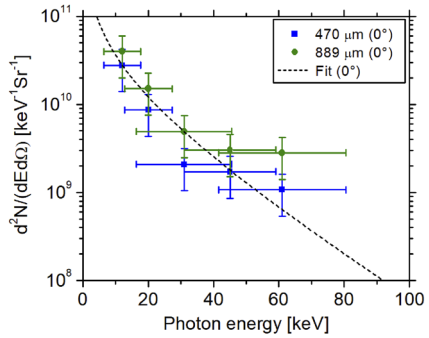

FIG. 15. X-ray spectra from shots evaluated with the help of the thick filters placed at 0° to the laser axis.

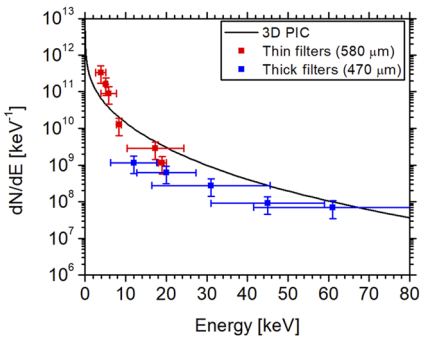

FIG. 16. Comparison of betatron radiation spectra from the experiments using thin filters (66 J, 580 μm foam) and thick filters (76 J, 470 μm) with the 3D-PIC simulation.

IV. CONCLUSION

The bright betatron radiation produced by direct laser-accelerated electrons in the interaction of the sub-ps PHELIX laser of ~10^{19} W/cm^2 intensity with pre-ionized low-density CHO foam targets was measured. To prevent interference of protons with the betatron radiation signal, we used optimized Mylar shielding. The impact of high-energy electrons (>30 MeV) on the measured betatron radiation signal has been corrected using a second IP layer (background monitor). Using sets of thin and thick filters, the absolute spectra of betatron radiation in the range of 5–60 keV were evaluated by the differential absorption method. With the help of two differential absorption spectrometers, we observed a relatively high directionality of the betatron radiation emission with FWHM of 14°–16°, which is narrower than in 3D-PIC simulations tailored for the PHELIX setup.[31] The total number of betatron photons with energy greater than 5 keV was experimentally determined to be 3×10^{11}, matching the simulation results. Thanks to the directional and efficient emission, the brilliance of betatron radiation at 5 keV is estimated to be as high as ~10^{21} photons s^{-1} mm^{-2} mrad^{-2} (0.1%BW)$^{-1}$. These values are comparable to the photon number and brilliance expected on PETAL in the self-modulated LWFA regime at a laser energy and intensity an order of magnitude higher than in the case of PHELIX.[28]

The combination of ultra-high photon fluence and high brilliance makes DLA-based betatron radiation sources very promising for high-energy-density research using kJ PW-class lasers.

ACKNOWLEDGMENTS

The results presented here are based on Experiment P207 performed at the PHELIX facility at the GSI Helmholtzzentrum für Schwerionenforschung, Darmstadt, Germany, in the framework of FAIR Phase-0 before 24 February 2022.

The authors are very grateful for the support provided by the PHELIX laser team. This research has been also supported by the Czech Ministry of Education, Youth and Sports (Project No. CZ.02.2.69/0.0/0.0/18_053/0016980) and the Grant Agency of the Czech Republic (Grant No. GM23-05027M).

AUTHOR DECLARATIONS

Conflict of Interest

The authors have no conflicts to disclose.

Author Contributions

J. Cikhardt: Conceptualization (equal); Data curation (equal); Formal analysis (equal); Funding acquisition (equal); Investigation (equal); Methodology (equal); Validation (equal); Visualization (equal); Writing – original draft (equal); Writing – review & editing (equal). **M. Gyrdymov**: Data curation (equal); Formal analysis (equal); Investigation (equal); Methodology (equal); Validation (equal). **S. Zähter**: Data curation (equal); Investigation (equal); Validation (equal). **P. Tavana**: Data curation (equal); Investigation (equal). **M. M. Günther**: Validation (equal). **N. Bukharskii**: Data curation (equal); Investigation (equal); Methodology (equal); Validation (equal). **N. Borisenko**: Data curation (equal); Investigation (equal). **J. Jacoby**: Validation (equal). **X. F. Shen**: Software (equal); Validation (equal). **A. Pukhov**: Software (equal); Validation (equal). **N. E. Andreev**: Validation (equal). **O. N. Rosmej**: Conceptualization (equal); Formal analysis (equal); Methodology (equal); Project administration (equal); Resources (equal); Supervision (equal); Validation (equal); Writing – review & editing (equal).

DATA AVAILABILITY

The data that support the findings of this study are available from the corresponding author upon reasonable request.

REFERENCES

[1] S. Corde, K. Ta Phuoc, G. Lambert *et al.*, "Femtosecond x rays from laser-plasma accelerators," Rev. Mod. Phys. **85**, 1 (2013).
[2] F. Albert, N. Lemos, J. L. Shaw *et al.*, "Betatron x-ray radiation in the self-modulated laser wakefield acceleration regime: Prospects for a novel probe at large scale laser facilities," Nucl. Fusion **59**, 032003 (2019).
[3] D. C. Swift, A. L. Kritcher, J. A. Hawreliak *et al.*, "Absolute Hugoniot measurements from a spherically convergent shock using x-ray radiography," Rev. Sci. Instrum. **89**, 053505 (2018).
[4] A. Ravasio, M. Koenig, S. Le Pape *et al.*, "Hard x-ray radiography for density measurement in shock compressed matter," Phys. Plasmas **15**, 060701 (2008).
[5] J. C. Wood, D. J. Chapman, K. Poder *et al.*, "Ultrafast imaging of laser driven shock waves using betatron x-rays from a laser wakefield accelerator," Sci. Rep. **8**, 11010 (2018).
[6] B. Mahieu, N. Jourdain, K. Ta Phuoc *et al.*, "Probing warm dense matter using femtosecond X-ray absorption spectroscopy with a laser-produced betatron source," Nat. Commun. **9**, 3276 (2018).
[7] J. M. Cole, J. C. Wood, N. C. Lopes *et al.*, "Laser-wakefield accelerators as hard x-ray sources for 3D medical imaging of human bone," Sci. Rep. **5**, 13244 (2015).
[8] A. Döpp, L. Hehn, J. Götzfried *et al.*, "Quick x-ray microtomography using a laser-driven betatron source," Optica **5**, 199–203 (2018).
[9] A. Rousse, K. T. Phuoc, R. Shah *et al.*, "Production of a keV -ray beam from synchrotron radiation in relativistic laser-plasma interaction," Phys. Rev. Lett. **93**, 135005 (2004).
[10] S. Kneip, C. McGuffey, F. Dollar *et al.*, "X-ray phase contrast imaging of biological specimens with femtosecond pulses of betatron radiation from a compact laser plasma wakefield accelerator," Appl. Phys. Lett. **99**, 093701 (2011).
[11] V. Horny, J. Nejdl, M. Kozlova *et al.*, "Temporal profile of betatron radiation from laser-driven electron accelerators," Phys. Plasmas **24**, 063107 (2017).
[12] A. Pukhov, Z.-M. Sheng, and J. Meyer-ter-Vehn, "Particle acceleration in relativistic laser channels," Phys. Plasmas **6**, 2847–2854 (1999).
[13] A. Pukhov, "Strong field interaction of laser radiation," Rep. Prog. Phys. **66**, 47–101 (2003).
[14] S. Kneip, S. R. Nagel, C. Bellei *et al.*, "Observation of synchrotron radiation from electrons accelerated in a petawatt-laser-generated plasma cavity," Phys. Rev. Lett. **100**, 105006 (2008).
[15] S. Fourmaux, S. Corde, K. T. Phuoc *et al.*, "Single shot phase contrast imaging using laser-produced Betatron x-ray beams," Opt. Lett. **36**, 2426–2428 (2011).
[16] J. Ju, K. Svensson, A. Döpp *et al.*, "Enhancement of x-rays generated by a guided laser wakefield accelerator inside capillary tubes," Appl. Phys. Lett. **100**, 191106 (2012).
[17] S. Cipiccia, M. R. Islam, B. Ersfeld *et al.*, "Gamma-rays from harmonically resonant betatron oscillations in a plasma wake," Nat. Phys. **7**, 867 (2011).
[18] M. Kozlova, I. Andriyash, J. Gautier *et al.*, "Hard x rays from laser-wakefield accelerators in density tailored plasmas," Phys. Rev. X **10**, 011061 (2020).
[19] J. P. Couperus, R. Pausch, A. Köhler *et al.*, "Demonstration of a beam loaded nanocoulomb-class laser wakefield accelerator," Nat. Commun. **8**, 487 (2017).

[20]C. Aniculaesei, T. Ha, S. Yoffe *et al.*, "The acceleration of a high-charge electron bunch to 10 GeV in a 10-cm nanoparticle-assisted wakefield accelerator," Matter Radiat. Extremes **9**, 014001 (2024).
[21]J. Götzfried, A. Döpp, M. F. Gilljohann *et al.*, "Physics of high-charge electron beams in laser-plasma wakefields," Phys. Rev. X **10**, 041015 (2020).
[22]J. Ferri, S. Corde, A. Döpp *et al.*, "High-brilliance betatron γ-ray source powered by laser-accelerated electrons," Phys. Rev. Lett. **120**, 254802 (2018).
[23]R. Rakowski, P. Zhang, K. Jensen *et al.*, "Transverse oscillating bubble enhanced laser-driven betatron X-ray radiation generation," Sci. Rep. **12**, 10855 (2022).
[24]N. E. Andreev, L. M. Gorbunov, V. I. Kirsanov *et al.*, "Resonant excitation of wake-fields by a laser pulse in a plasma," JETP Lett. **55**, 571–576 (1992).
[25]N. E. Andreev, V. I. Kirsanov, L. M. Gorbunov *et al.*, "Stimulated processes and self-modulation of a short intense laser pulse in the laser wake-field accelerator," Phys. Plasmas **2**(6), 2573–2582 (1995).
[26]E. Esarey, C. B. Schroeder, and W. P. Leemans, "Physics of laser-driven plasma-based electron accelerators," Rev. Mod. Phys. **81**, 1229 (2009).
[27]F. Albert, N. Lemos, J. L. Shaw *et al.*, "Observation of betatron x-ray radiation in a self-modulated laser wakefield accelerator driven with picosecond laser pulses," Phys. Rev. Lett. **118**(13), 134801 (2017).
[28]J. Ferri, X. Davoine, S. Y. Kalmykov, and A. Lifschitz, "Electron acceleration and generation of high-brilliance x-ray radiation in kilojoule, subpicosecond laser-plasma interactions," Phys. Rev. Accel. Beams **19**, 101301 (2016).
[29]A. Pukhov, "Three-dimensional electromagnetic relativistic particle-in-cell code VLPL (Virtual Laser Plasma Lab)," J. Plasma Phys. **61**(3), 425–433 (1999).
[30]B. Williamson, G. Xia, S. Gessner *et al.*, "Betatron radiation diagnostics for AWAKE Run 2," Nucl. Instrum. Methods Phys. Res., Sect. A **971**, 164076 (2020).
[31]X. F. Shen, A. Pukhov, M. M. Gunther, and O. N. Rosmej, "Bright betatron x-rays generation from picosecond laser interactions with long-scale near critical density plasmas," Appl. Phys. Lett. **118**, 134102 (2021).
[32]O. N. Rosmej, X. F. Shen, A. Pukhov *et al.*, "Bright betatron radiation from direct-laser-accelerated electrons at moderate relativistic laser intensity," Matter Radiat. Extremes **6**, 048401 (2021).
[33]R. Jung, J. Osterholz, K. Löwenbrück *et al.*, "Study of electron-beam propagation through preionized dense foam plasmas," Phys. Rev. Lett. **94**, 195001 (2005).
[34]L. Willingale, S. R. Nagel, A. G. R. Thomas *et al.*, "Characterization of high-intensity laser propagation in the relativistic transparent regime through measurements of energetic proton beams," Phys. Rev. Lett. **102**, 125002 (2009).
[35]L. Willingale, P. M. Nilson, A. G. R. Thomas *et al.*, "High-power, kilojoule laser interactions with near-critical density plasma," Phys. Plasmas **18**, 056706 (2011).
[36]L. Willingale, A. V. Arefiev, G. J. Williams *et al.*, "The unexpected role of evolving longitudinal electric fields in generating energetic electrons in relativistically transparent plasmas," New J. Phys. **20**, 093024 (2018).
[37]O. N. Rosmej, N. E. Andreev, S. Zaehter *et al.*, "Interaction of relativistically intense laser pulses with long-scale near critical plasmas for optimization of laser based sources of MeV electrons and gamma-rays," New J. Phys. **21**, 043044 (2019).
[38]O. N. Rosmej, M. Gyrdymov, M. M. Günther *et al.*, "High-current laser-driven beams of relativistic electrons for high energy density research," Plasma Phys. Controlled Fusion **62**, 115024 (2020).
[39]M. Günther, O. N. Rosmej, P. Tavana *et al.*, "Forward-looking insights in laser-generated ultra-intense γ-ray and neutron sources for nuclear application and science," Nat. Commun. **13**, 170 (2022).
[40]P. Tavana, N. Bukharskii, M. Gyrdymov *et al.*, "Ultra-high efficiency bremsstrahlung production in the interaction of direct laser-accelerated electrons with high-Z material," Front. Phys. **11**, 1178967 (2023).
[41]L. P. Pugachev, N. E. Andreev, P. R. Levashov, and O. Rosmej, "Acceleration of electrons under the action of petawatt-class laser pulses onto foam targets," Nucl. Instrum. Methods Phys. Res., Sect. A **829**, 88–93 (2016).
[42]N. G. Borisenko, A. M. Khalenkov, V. Kmetik *et al.*, "Plastic aerogel targets and optical transparency of undercritical microheterogeneous plasma," Fusion Sci. Technol. **51**, 655–664 (2007).
[43]V. Bagnoud, B. Aurand, A. Blazevic *et al.*, "Commissioning and early experiments of the PHELIX facility," Appl. Phys. B **100**, 137–150 (2010).
[44]P. A. Ross, "A new method of spectroscopy for faint X-radiations," J. Opt. Soc. Am. **16**, 433–437 (1928).
[45]P. Kirkpatrick, "On the theory and use of Ross filters," Rev. Sci. Instrum. **10**, 186–191 (1939).
[46]Center for X-Ray Optics is a multi-disciplined research group within Lawrence Berkeley National Laboratory's, https://henke.lbl.gov/optical_constants/.
[47]B. L. Henke, E. M. Gullikson, and J. C. Davis, "X-ray interactions: Photoabsorption, scattering, transmission, and reflection at E = 50-30 000 eV, Z = 1-92," At. Data Nucl. Data Tables **54**(2), 181–342 (1993).
[48]T. Weingartner, The x-ray transmission calculator, https://calc.weingos.com/.
[49]AXUV HS11 Photodiode datasheet, Opto Diode Corporation, www.optodiode.com, Revision November 26, 2019.
[50]K. S. Bell, C. A. Coverdale, D. J. Ampleford *et al.*, "The differential absorption hard x-ray spectrometer at the Z facility," IEEE Trans. Plasma Sci. **45**, 2393–2398 (2017).
[51]G. Boutoux, D. Batani, F. Burgy *et al.*, "Validation of modelled imaging plates sensitivity to 1-100 keV x-rays and spatial resolution characterisation for diagnostics for the 'PETawatt Aquitaine Laser,'" Rev. Sci. Instrum. **87**, 043108 (2016).
[52]B. Kindler, E. Celik Ayik, A. Hübner *et al.*, "Surface and thickness measurement in the Targetlab of GSI," EPJ Web Conf. **229**, 02002 (2020).
[53]V. Munzar, D. Klir, J. Cikhardt *et al.*, "Investigation of magnetic fields in Z-pinches via multi-MeV proton deflectometry," IEEE Trans. Plasma Sci. **46**, 3891–3900 (2018).
[54]T. Bonnet, M. Comet, D. Denis-Petit *et al.*, "Response functions of imaging plates to photons, electrons and ^{4}He particles," Rev. Sci. Instrum. **84**, 103510 (2013).
[55]J. Sempau, E. Acosta, J. Baro *et al.*, "An algorithm for Monte Carlo simulation of coupled electron-photon transport," Nucl. Instrum. Methods Phys. Res., Sect. B **132**, 377–390 (1997).
[56]B. R. Maddox, H. S. Park, B. A. Remington *et al.*, Rev. Sci. Instrum. **82**, 023111 (2011).
[57]W. Nakel, Phys. Rep. **243**(6), 317–353 (1994).
[58]E. Esarey, B. A. Shadwick, P. Catravas, and W. P. Leemans, "Synchrotron radiation from electron beams in plasma-focusing channels," Phys. Rev. E **65**, 056505 (2002).
[59]S. Kneip, C. McGuffey, J. L. Martins *et al.*, "Bright spatially coherent synchrotron X-rays from a table-top source," Nat. Phys. **6**, 980–983 (2010).
[60]S. Fourmaux, E. Hallin, U. Chaulagain *et al.*, "Laser-based synchrotron X-ray radiation experimental scaling," Opt. Express **28**(3), 3147–3158 (2020).